Journal of Photochemistry & Photobiology, B: Biology 190 (2019) 128–136

Contents lists available at ScienceDirect

Journal of Photochemistry & Photobiology, B: Biology

journal homepage: www.elsevier.com/locate/jphotobiol

Cationic red emitting fluorophore: A light up NIR fluorescent probe for G4-DNA

Beena Kumari[a], Akanksha Yadav[b], Sushree P. Pany[b], Pradeepkumar P.I.[b,*], Sriram Kanvah[a,*]

[a] Department of Chemistry, Indian Institute of Technology Gandhinagar, Palaj, Gandhinagar 382 355, India
[b] Department of Chemistry, Indian Institute of Technology Bombay, Powai, Mumbai 400 076, India

ARTICLE INFO

Keywords:
G4-quadruplexes
NIR fluorescence
Styrylpyridinium dyes
Solvatochromism

ABSTRACT

Guanine (G) quadruplexes (G4) are nucleic acid secondary structures formed by G-rich sequences, commonly found in human telomeric and oncogene-promoter regions, have emerged as targets for regulation of multiple biological processes. Considering their importance, targeting the G-quadruplex structure with small molecular binders is extremely pertinent. In this work, red emitting water soluble fluorophores bearing push-pull substituents were synthesized and examined for their interaction with human telomeric G4 and duplex (ds) -DNAs. The presence of a strong electron donating (dimethylamino) and electron withdrawing (cationic pyridinium) groups linked through a conjugated double bond helps in water solubility and enabling the emission in the near IR region (> 700–nm). Binding of this cationic dye to the G4-DNA yields multiple-fold emission enhancement (~70 fold with G4-DNA *vs.* ~7 fold with ds-DNA) along with hypsochromic wavelength shifts (35 nm with G4-DNA and 8 nm with ds-DNA). The remarkable emission changes, ~2–4 fold enhanced binding efficiency noted with the antiparallel conformation of G4-DNA indicates preferential selectivity over ds-DNA. The molecular docking and dynamics studies of the ligands with duplex and G4-DNA were performed, and they provide insights into the mode of binding of these dyes with G4-DNA and supplement the experimental observations.

1. Introduction

Guanine quadruplexes (G4) are secondary DNA structures composed of planar Hoogsteen- paired G tetrad structures. In the presence of suitable monovalent metal ions such as sodium or potassium, the G-quartets stack on top of each other yielding four-stranded structures [1]. Several studies have linked the formation of G4 structures *in vivo* with biological processes such as gene expression, transcription, and telomerase inhibition [2–5]. Stabilization and selective recognition of G4 structures over duplex DNA (ds-DNA) by using small molecular ligands is thus an attractive area of interest [6–8]. Such recognition approach using small fluorescent molecules have found significant interest in analytical biochemistry and medicine [9]. Typically these probes show a strong fluorescence signal (light-up) upon binding the biomolecule of interest. Considering their efficiency, newer fluorescence probes that exhibit such enhanced emission are sought for detection of biomacromolecules [10,11]. Previously known probes that show G4 binding as well as fluorescence/luminescence light-up properties include Ru (II) metallopeptides [12], antibodies [13], thioflavin-T [13,14], pyrenyl derivatives [15], cyanine dyes [16], isaindigotones [17], styryl coumarin dyes with quinoline or quinazolinium [18,19], benzothiazole dyes [20], and triphenylamine derivatives [21,22]. Several other ligands and molecules were also reported for their selective stabilization towards G4-DNA over ds-DNAs [23]. However, it is still challenging to develop novel small molecular ligands for selective recognition of the G4-DNA along with emission in the red region.

In this work, we designed the fluorophores with an intention to create probes having water solubility, show emission in the red region, and capable of interaction with the nucleic acid structures. Naphthalene derivatives have been used as stabilizers for the G4-DNA nucleic acids structures [24–28], as the DNA “base” equivalent [29] and for biological imaging [30–32]. The presence of donor and acceptor substituents induces strong intramolecular charge transfer (ICT) yielding the absorption and emission in the longer wavelength regions, and the presence of charged groups may help in water solubility. With this strategy, we designed fluorophores bearing naphthalene moiety, bearing a donor group in the form of dimethylamine, a charged and electron withdrawing group in the form of the pyridinium group (Scheme 1). It is expected that the naphthalene scaffold assists in stacking interactions with G-quartet, the cationic groups assist in electrostatic interactions apart from improving the water solubility and the push-pull substituents yield emission greater than > 650 nm. The

* Corresponding authors.
E-mail addresses: pradeep@chem.iitb.ac.in (P.I. Pradeepkumar), kanvah@gmail.com (S. Kanvah).

https://doi.org/10.1016/j.jphotobiol.2018.10.007
Received 14 August 2018; Received in revised form 18 September 2018; Accepted 6 October 2018
Available online 11 October 2018
1011-1344/ © 2018 Published by Elsevier B.V.

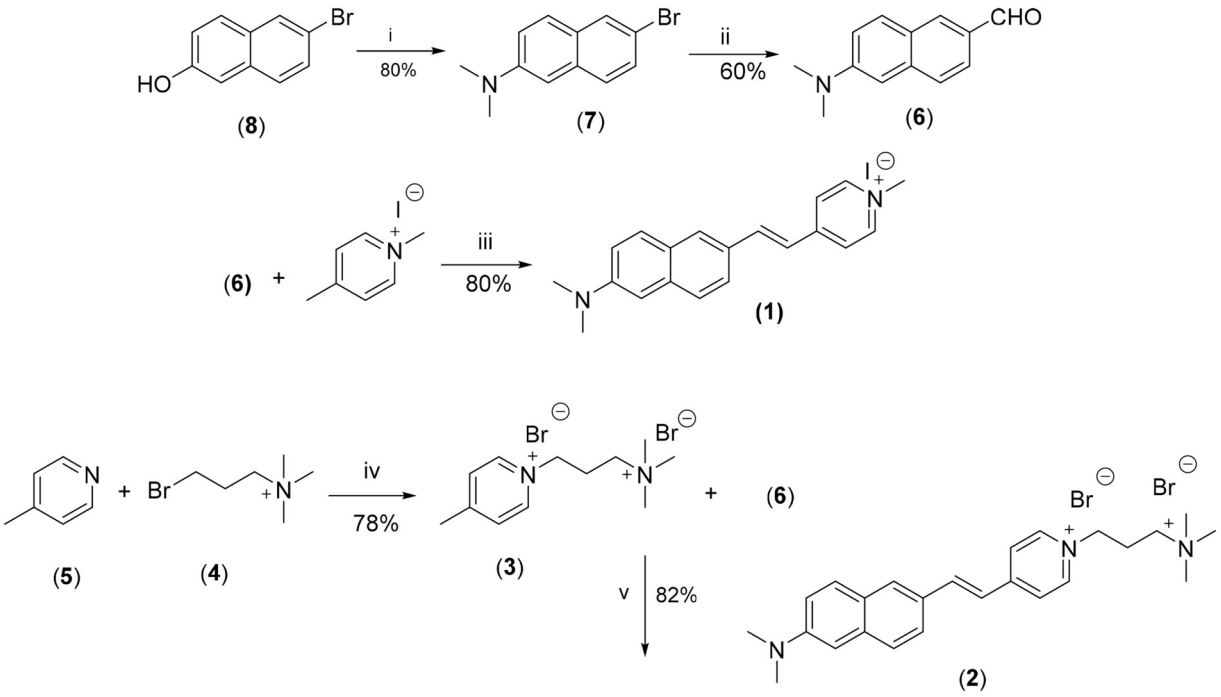

Scheme 1. Synthetic route used to obtain the pyridinium derivatives. Reagents and conditions: i) $Na_2S_2O_5$, $NHMe_2$, H_2O, 140 °C, 48 h; ii) n-BuLi, DMF, THF, −78 °C, 8 h; iii) Piperidine, $Zn(OAc)_2$, ethanol, 80 °C, 3 h; iv) DMF, 100 °C, 7 h; v) Piperidine, ethanol, 100 °C, 12 h.

synthesis, absorption and emission studies and the binding interaction, stability and selectivity of these ligands towards G4-DNA and duplex (ds) DNAs have been explored by various biophysical methods such as CD titration, CD melting, fluorescence. The results are rationalized by using molecular docking and molecular dynamics simulations.

2. Experimental Section

The chemicals that were used for the synthesis and studies were purchased from Sigma Aldrich, S. D. Fine, Alfa Aesar and Acros. UV–V is absorption spectra were recorded using Analytik Jena Specord 210 plus or Perkin Elmer Lambda Bio + UV spectrophotometers. Synthesized samples were characterized using 500 MHz Bruker Avance NMR spectrometer. Mass spectral data were obtained using the Waters-Synapt G2S high-resolution mass spectrometer [ESI-QToF] equipped with UPLC. The DNA oligomers 22AG (5′-AGGGTTAGGGTTAGGGTTA GGG-3′) and ds-DNA (5′-GGGTTACTACGAACTGG-3′ and its complementary strand 3′CCCAATGATGCTTGACC-5′) purchased from Xcelris Labs were purified using denaturing PAGE (20%, 7 M urea), followed by excision and desalting by Sep-Pak column. The DNA concentration was measured at 260 nm using the appropriate molar absorption coefficients (ε). For biophysical experiments, the ligand **1** was prepared in DMSO (5 mM), and the ligand **2** was prepared in water (5 mM).

3. Fluorimetric Titration Studies

The fluorescence emission studies were carried out using Horiba-Jobin Yvon Fluolorog-3 spectrofluorometer and Fluoromax- 4 spectrofluorometers at the excitation wavelength of 450 nm for the synthesized fluorophores. Fluorimetric titration was performed using a 100 µL quartz cuvette having a 1 cm path length. The quadruplex and duplex DNA of 100 µM concentration were prepared in 100 mM sodium chloride solution and 10 mM lithium cacodylate buffer (pH 7.4). To make ds or G4-DNA structures, DNA oligomers were annealed by heating at 95 °C for 5 min followed by gradual cooling to room temperature for 3–4 h. A fixed concentration (10 µM) of the dye was titrated with increasing concentration of the DNA (12 to 18 µM) at an excitation wavelength of 450 nm. The solution was allowed to saturate for 3 min post addition of DNA to the dye solution before recording the emission spectra. The normalized emission spectra were plotted against the logarithm of the concentration of ligand, and the curve fitting was carried out using the nonlinear regression obeying Hill equation (Eq. (1)).

$$F_N = F_0 + (F_s - F_0)\left(\frac{[DNA]^n}{[K_d]^n + [DNA]^n}\right) \quad (1)$$

F_N, the normalized fluorescence intensity, F_0 is the intensity in the absence of DNA, F_s is the maximum fluorescence intensity upon saturation, n is the number of cooperative binding sites, and K_d is the dissociation constant ($1/K_a$).

4. CD melting and Titration Experiments

Circular dichroism (CD) spectra were recorded at room temperature on a JASCO J-815 spectrophotometer. DNA solutions (10 µM G4-DNA and 15 µM ds-DNA) were prepared in 10 mM lithium cacodylate buffer in the presence of 50 mM NaCl, at pH 7.4. DNA samples were annealed at 95 °C for 5 min and allowed to cool down to room temperature. After addition of 5 equivalents of dye (50 µM, 75 µM for G4 and ds-DNA respectively) into the DNA, the solution was allowed to incubate overnight. The melting temperature (T_m) curves were recorded from 20 °C to 95 °C with an increment of 1 °C/min. As the ionic strength is known to modulate the binding of the cationic ligand to the negatively charged DNA, for all melting experiments, the total ionic strength of 110 mM was maintained with the help of Li^+ ions, which does not alter the structure and stability of the Na^+ induced G4-DNA. The spectra were recorded from 200 to 500 nm with a scanning speed of 100 nm/min in 1 mm path length quartz cuvette. The baseline correction was done using NaCl, Lithium cacodylate buffer [pH 7.4]. All the spectra were collected as an average of three measurements.

5. Molecular Modelling and Dynamics Studies

To understand the binding modes, stability and interactions of the ligands with the G4-DNA, docking studies, molecular dynamics, and binding energy evaluation were carried out. [33] Coordinates for the anti-parallel telomeric G4-DNA (PDB:143D) were obtained in the same way as described previously [34]. Ligand structures were constructed using GaussView 5.0 and optimized using the HF/6-311 + G(d,p) basis set on the R.E.D server [35] which uses Gaussian 09. Docking studies were performed using the Lamarckian genetic algorithm in Autodock 4.2 [36].The optimized structure of ligands was used to perform rigid docking of the ligand with G4-DNA. The PDB file was modified for docking purposes [34]. A grid space spanning the entire DNA was constructed and the ligand was randomly placed inside it. Default parameters in Autodock 4.2 were used to generate 250 independent docked conformations. Clustering of the docked conformations with RMSD 0.5, 1.0, 2.0 and 3.0 Å was performed, and accordingly, a representative structure of a cluster with a maximum number of conformations was chosen for further analysis.

To prepare the systems for subsequent MD studies, the generalized AMBER force field (GAFF) [37] and ff09bsc0 [38] were used to parameterize the ligand and DNA respectively. Restrained electrostatic potential (RESP) [39] charges were obtained by calculating the electrostatic potential using Gaussian 09 followed by charge assignment using Antechamber module of AMBER 14 [40]. Further, the DNA and ligand docked complex was solvated using TIP3P water molecules extending to a size of 10 Å in a truncated octahedron. K^+ ions were added to neutralize the system. The solvated system was subjected to 10,000 steps of minimization holding the DNA and ligand restraint followed by 5000 steps of unrestrained steepest descent minimization, 100 ps of heating to 300 K using Langevin dynamics, 100 ps of density equilibration which was finally followed by 100 ns of unrestrained dynamics with coordinates saved for every 2 ps. The time step for the run was 2 fs, and it was carried out using the GPU accelerated version of PMEMD in AMBER 14 [41,42]. The binding free energies were calculated using the MM-PBSA method [43] (MMPBSA.py module in AMBER 14) for the last 50 ns. Every 5th frame was sampled from the final trajectory which accounts for a total of 5000 frames considered for the binding energy calculations. RMSD of heavy atoms of backbone, ligand atoms, and G-quartet atoms, RMSF values of DNA residues. Hoogsteen H-bond occupancies every calculated for every 5th frame (10 ps) using the CPPTRAJ [44] module in AMBER 14. For defining the H-bond, a distance cut-off of 3.5 Å between heavy atoms was used. Every 50th frame and a total of 1000 frames were considered for the calculation of stacking distances and angles. To visualize and analyze the MD trajectories, UCSF Chimera [45] was used. PyMOL (http://www.pymol.org) was used to visualize the structures and generate the images.

6. Synthetic Procedures

6.1. 6-Bromo-2-Dimethylaminonaphthalene (7) [46]

A mixture containing dimethylamine (50% in H_2O, 4 mL, 44.85 mmol), 6-bromo-2-naphthol (2.0 g, 8.97 mmol), $Na_2S_2O_5$ (3.57 g, 17.94 mmol), and H_2O (20 mL) in a sealed tube was stirred at 145 °C for 48 h. The product obtained was collected by filtration, washed with water, and the combined filtrate was extracted with methylene chloride and purified by column chromatography to afford **7** (white solid, 1.72 g, 65.8%).

^{1}H NMR (500 MHz, $CDCl_3$): δ 7.86 (s,1H), 7.64–7.63 (d, J = 9 Hz, 1H), 7.56–7.54 (d, J = 9 Hz, 1H), 7.46–7.44 (d, J = 8.5 Hz, 1H), 7.29 (s, 1H), 7.20–7.19 (s, J = 8.5 Hz, 1H), 6.89 (s,1H) 3.08 (s, 6H); ^{13}C NMR (125 MHz, $CDCl_3$): δ 130.7, 130.0, 128.9, 127.7, 126.7, 126.7, 126.6, 125.5, 123.8, 120.7, 116.5, 106.4, 96.1, 77.2, 76.9, 76.7.

6.2. 6-Formyl-2-Dimethylaminonaphthalene (6) [47]

Compound **8** (1.5 g, 6.0 mmol) was dissolved in THF (15 mL) and cooled to −78 °C under N_2 atmosphere. 1.6 M BuLi in hexane (0.8 mL, 7.2 mmol) was added at −78 °C to the reaction contents and stirred for 30 min. This is followed by addition of DMF (7.2 mmol) and the reaction was warmed upto 0 °C. Progress of the reaction was monitored by TLC and upon completion, the reaction was quenched with water. The contents were extracted with dichloromethane, and the desired product was purified through silica-gel column chromatography (ethyl acetate/hexane (5/95, v/v) as eluent) to yield **6** (yellow solid, 1.0 g, 85%).

^{1}H NMR (500 MHz, $CDCl_3$): δ 10.03 (s,1H), 7.64–7.63 (d, J = 9 Hz, 1H), 7.56–7.54 (d, J = 9 Hz, 1H), 7.46–7.44 (d, J = 8.5 Hz, 1H), 7.20–7.19 (d, J = 9 Hz, 1H), 6.89 (s, 1H), 3.08 (s, 6H); ^{13}C NMR (125 MHz, $CDCl_3$): δ 191.8, 150.6, 138.6, 134.7, 130.7, 130.6, 126.8, 125.0, 123.5, 116.2, 105.4, 77.3, 77.0, 76.8, 40.3.

6.3. 4 Methyl-1-(3-(trimethyl ammonia)propyl) Pyridine-1-ium Bromide (3) [48]

A mixture of 4-methyl pyridine (15.3 mmol, 1.49 mL) and 3-Bromo-*N*,*N*,*N*-trimethylpropan-1-aminium (7.7 mmol, 1.39 g) in DMF was heated at 100 °C for 7 h. After cooling down to room temperature, the solution was concentrated under reduced pressure. Ethyl acetate was added and the suspension was stirred at room temperature for 8 h. The precipitate was collected by centrifugation and dried to a constant weight to give compound 3 (off-white solid, 1.41 g, Yield 80%).

^{1}H NMR (500 MHz, $CDCl_3$): δ 8.69–8.68 (d, J = 6 Hz, 2H), 7.91–7.90 (d, J = 6.0 Hz, 2H), 4.66–4.63 (t, 2H), 3.51–3.48 (m, 2H), 3.15 (s, 9H), 2.64 (s, 3H), 2.59–2.53 (m, 2H), 3.08 (s, 6H); ^{13}C NMR (125 MHz, $CDCl_3$): δ 159.7, 141.4, 129.8, 62.1, 136.4, 57.3, 52.9, 24.7, 21.9.

6.4. (E)-4-(2-(6-(dimethylamino) naphthalene-2-yl)vinyl)-1-Methylpyridin-1-ium Iodide (1)

To a mixture of 1-methyl-4-pyridinium iodide (2.9 mmol, 0.7 g) and **6** (2.9 mmol, 0.59 g) in piperidine (~2–3 drops), zinc acetate (0.1 mmol, 0.03 g) in 20 mL of absolute ethanol was added and the contents were heated at 80 °C. The deep-red colored mixture obtained was cooled to room temperature yielding a red precipitate of **1** (0.42 g, yield 67%).

^{1}HNMR (500 MHz, DMSO-d_6): δ 8.79–8.78 (d, J = 6.5 Hz, 2H), 8.16–8.15 (d, J = 6.5 Hz, 2H), 4.66–4.63 (t, J = 15 Hz, 2H) 3.51–3.48 (m, J = 15 Hz, 2H), 3.15 (s, 9H), 2.64 (s, 3H), 2.59–2.53 (m, 2H), 3.08 (s, 6H); ^{13}C NMR (125 MHz, DMSO-d_6): δ 153.5, 150.0, 145.2, 142.0, 136.4, 130.6, 130.1, 128.8, 127.2, 125.9, 124.4, 123.4, 121.1, 117.0, 105.8, 47.8. HRMS: calcd for $C_{20}H_{21}N_2^+$ $[M]^+$ 290.1700; found $[M]^+$ 290.1710 (error = 3.45 ppm).

6.5. (E)-4(2-(6-(dimethyl amino) napthalen-2-yl)vinyl)-1-(3-trimethyl ammonia)propyl Pyridine (2)

Compound **6** (0.290 g, 1.45 mmol) and quaternary ammonium salt (0.283 g, 1.46 mmol) was added to a dry round bottomed flask in the presence of N_2. To this, ethanol (10 mL) followed by piperidine (2–3 drops) were added and the contents were refluxed for 12 h at 100 °C. Solvent was evaporated under reduced pressure and the desired compound (**2**) is obtained by precipitation in ethanol (dark red solid, 0.15 g, Yield 51%).

^{1}H NMR (500 MHz, CD_3OD): δ 8.70–8.69 (d, J = 7 Hz, 2H), 8.08–8.07 (d, J = 6.5 Hz, 2H,), 7.99–7.96 (1 s, J = 16 Hz, 1H), 7.88 (s, 1H), 7.68–7.66 (d, J = 9 Hz, 1H) 7.27–7.23 (d, J = 20 Hz, 1H), 6.62–6.60 (d, J = 10 Hz, 1H) 6.35 (s, 1H), 4.54–4.51 (t, J = 7.5 Hz, 2H), 3.49–3.46 (t, J = 7.5 Hz, 2H), 3.29–3.28 (q, J = 5 Hz, 4H), 2.52 (m, 2H) 1.09–1.07 (t, J = 5 Hz, 3H).

^{13}C NMR (125 MHz, CD_3OD,): δ 162.6, 156.1, 154.6, 152.7, 145.4, 143.3, 136.6, 123.7, 121.6, 112.4, 110.9, 108.9, 96.3, 62.3, 56.6, 53.2, 44.9, 24.5, 11.9. HRMS: calcd for $C_{25}H_{33}N_3^{2+}$ $[M/2]^+$ 187.1293; found $[M/2]^+$ 187.1301 (error = 4.27 ppm).

7. Results and Discussion

7.1. Ligand Design and Synthesis

The push-pull substituted naphthalene derivatives have been used as excellent staining dyes for various biological applications due to their ability to cross the blood-brain barrier [49]. The fluorophores (**1** and **2**) were synthesized based on the synthetic route given in Scheme 1. The reaction of bromonapthol **8** with dimethylamine ($NHMe_2$) and sodium metabisulfite ($Na_2S_2O_5$) yielded dimethylaminobromonapthalene derivative (**7**) [50]. The dimethylaminonaphthaldehyde **6** was obtained on the reaction of **7** with BuLi and DMF at −78 °C [51]. The ligand **1** was obtained by reaction of **6** with 4-methylpyridinium cation with piperidine, zinc acetate [52]. The reaction of 4-methylpyridine **5** with (3-Bromopropyl) trimethylammonium bromide **4** yielded the dicationic 4-methylpyridinium derivative **3** which on subsequent condensation with aldehyde **6** in the presence of piperidine yielded the desired ligand **2** [48].

7.2. Absorption and Emission Studies

Ligand **1** absorbs at ~464 nm in dioxane and shows weak bathochromic emission shifts (9 nm) with an increase in solvent polarity (473 nm in methanol) (Fig. 1). However, in water, ligand **1** shows a hypsochromic shift of 45 nm. The ligand **2**, having the same chromophore, absorbs at 465 nm in dioxane and the absorption maxima shifts to lower energy (420 nm in water) with an increase in solvent polarity. The shifts in absorption are greater for **2** than for **1** due to the presence of additional quaternary ammonium group. This additional positive charge will cause perturbations to the solute-solvent dipole interactions resulting in the observed bathochromic absorption shifts [53]. Like in **1**, ligand **2** also shows a strong hypsochromic absorption shift (48 nm) in water. This hypsochromic shift in water is due to charge stabilization of the positively charged cations with water (Fig. 1).

Ligand **1** exhibits strong solvatochromic emission shifts [~ +90 nm] with change in solvent polarity [Fig. 2]. In dioxane, the emission is noted at 638 nm and in polar solvents emission is red-shifted with emission in the range of 730–736 nm. The emission band observed at lower wavelength band is due to locally excited species and the emission at a longer wavelength is due to the charge transfer (CT) band. In strongly polar solvents the CT band remains conspicuous. Ligand **2** shows similar trends with emission at 677 nm in dioxane with a shoulder band at ~560 nm. In polar solvents, the emission is quenched with emission maxima at 743–757 nm [Fig. 2]. In water, the emission is weak, but the emission maximum is centred about ~758 nm. Similar to the absorption trend, the ligand **2** emits at slightly longer emission wavelengths [+21 nm] compared to the ligand **1** in H_2O. This is attributed to the presence of additional quaternary ammonium cation leading to greater excited state charge stabilization resulting in bathochromic emission shifts [53].

7.3. CD Melting Studies

The synthesized fluorophores have two important characteristics i) emission > 650 nm and ii) the water solubility due to the presence of cationic groups. The presence of cationic groups favor interaction with substrates such as DNA bearing negatively charged phosphate groups. With these advantages in mind, we studied their interaction with a telomeric G4-DNA and a 17-mer duplex DNA (ds-DNA). Their thermal stability (T_m) was studied by monitoring the melting process by at 260 nm and 295 nm for ds-DNA and G4- DNA respectively. [Fig. 3] Native G4-DNA melts at 51.1 °C and the corresponding T_m for ds-DNA was 53.3 °C. Addition of the ligands yield 2–8 °C rise with G4-DNA, but the effects on ds-DNA is found to be less (1–2 °C) [Fig. 3]. The increased melting indicates greater stability of the DNA structures in the presence of these cationic ligands.

7.4. CD Titration Studies

To further understand the influence of added dye on the DNA structure, CD titration experiments were carried out. The G4-strands can adopt different topologies such as parallel, antiparallel structures depending on G-tetrad stacking, cations or the presence of small molecules [1,54]. In the presence of NaCl, the CD spectra show positive peaks at ~292 nm, 245 nm and a negative peak at 262 nm [Fig. 4]. These are characteristic peaks of anti-parallel topology. After the addition of the ligands **1** and **2**, no significant changes were noted, and the anti-parallel topology of G4-DNA is preserved.

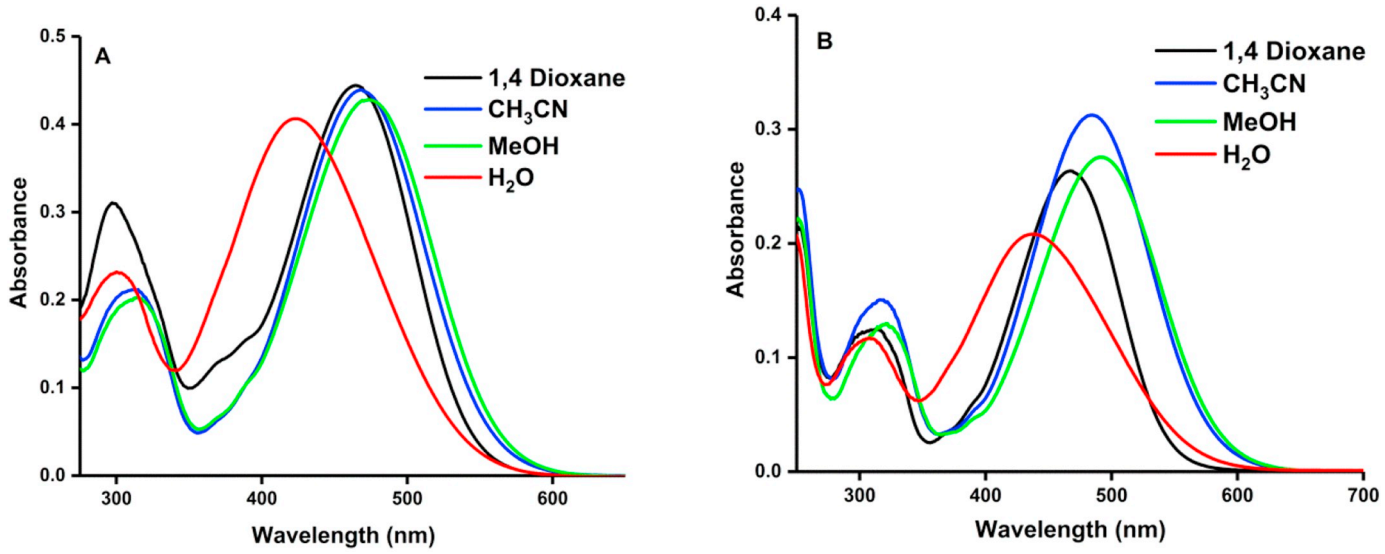

Fig. 1. Absorption spectra of 10 μM of (A) ligand **1** and (B) ligand **2** in different solvents.

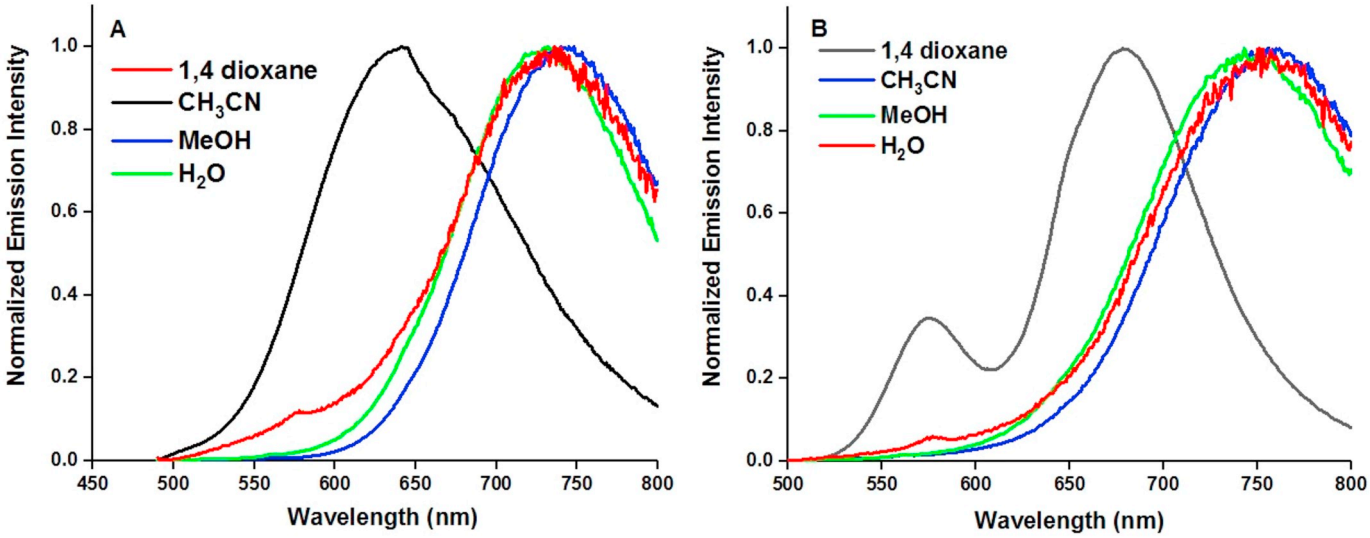

Fig. 2. Emission of 10 μM of (A) ligand **1** and (B) ligand **2** in different solvents.

7.5. Fluorescence Emission Studies

The titration of ligand **1** with increasing concentration of ds-DNA resulted in gradual enhancement of ligand fluorescence [~4.6 fold enhancement] together with a hypsochromic shift (20 nm) [Fig. S1A]. Ligand **2** shows emission at ~758 nm and the addition of ds-DNA results in ~9 fold enhancement in intensity with concomitant hypsochromic emission shifts (25 nm) [Fig. S1B]. These emission changes indicate slightly stronger binding preference of the ligand **2** over the ligand **1** with ds-DNA. With G4-DNA, ligand **1** shows a ~32-fold emission intensity enhancement with ~35 nm hypsochromic shift in emission wavelength [Fig. 5A]. Ligand **2** leads to a ~73 fold intensity enhancement with a ~43 nm blue-shift in emission wavelength [Fig. 5B]. Indeed, the ligand **2** bearing two cationic groups shows stronger binding affinity with both duplex and G4-DNA. A comparative plot of the change in emission intensity with added DNA concentration is shown in Fig. 5C. The dissociation constant calculated for G4-DNA with ligands **1** and **2** are $[5.5 \pm 0.1 \times 10^{-6}\,M]$ and $[5.01 \pm 0.05 \times 10^{-6}\,M]$ respectively. The corresponding values for ds-DNA of **1** and **2** are found to be $[11.4 \pm 1.59 \times 10^{-6}\,M]$ and $[20.8 \pm 0.23 \times 10^{-6}\,M]$ respectively (Fig. S2 and Table S1). These values reveal ~ 2 fold [ligand **1**], and ~4 fold [ligand **2**] increased binding efficiency of these ligands with G4-DNA over ds-DNA. The low dissociation constants coupled with enhanced emission intensities of ligands indicate preferential binding of these molecules towards G4-DNA.

7.6. Molecular Modelling and Dynamics Studies

To probe the possible binding modes and interactions of ligands **1** and **2** with G4-DNA, molecular modelling, and dynamics simulations were carried out using antiparallel human telomeric G4 (PDB:143D) DNA structure [55]. The energy optimized structures of ligands **1** and **2** [Figs. S3 and S4] generated at the HF/6-311 + G(d,p) theory level were utilized for docking with telomeric DNA structure using Autodock 4.2. Docking results showed that both the ligands preferentially stack between the top quartet and the diagonal loop (pseudo intercalation site) of the antiparallel G4-DNA. Utilizing each of these docked complexes, two systems were prepared, each of which was subjected to a final MD run of 100 ns using GPU accelerated version of PMEMD in AMBER 14 [41].

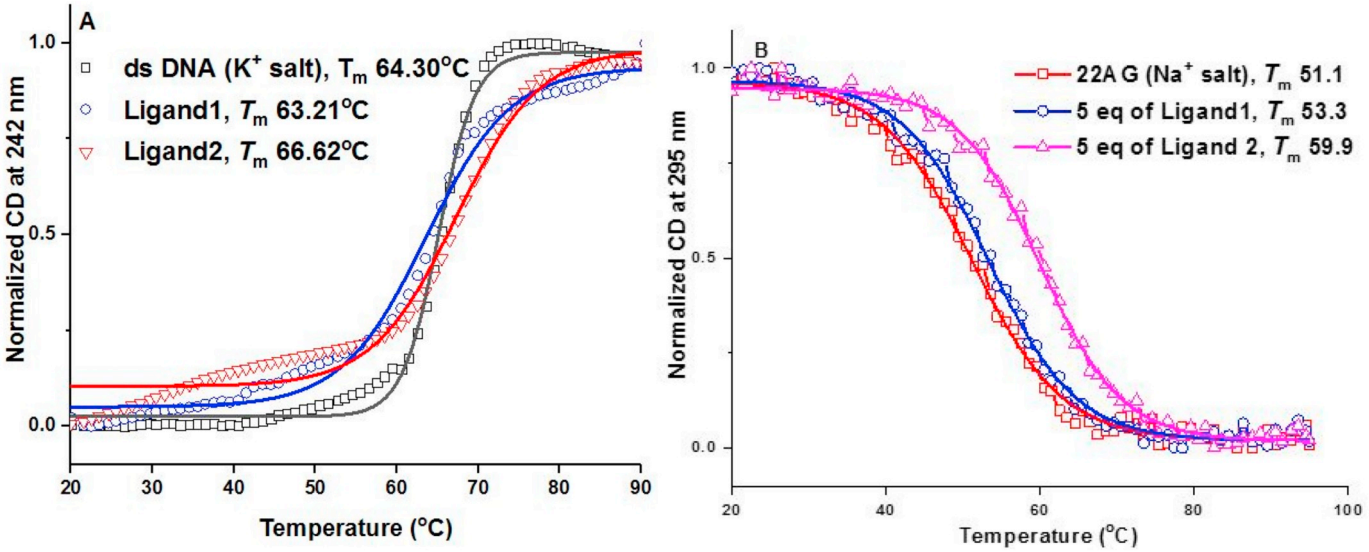

Fig. 3. CD melting spectra of ligands **1** and **2** with dsDNA (15 μM) and the quadruplex DNAs (10 μM) in 10 mM lithium cacodylate buffer, pH 7.2 in the absence and in the presence of 5 equiv. of ligands. (A) Duplex DNA (10 mM KCl and 90 mM LiCl); and (B) Telomeric DNA (10 mM NaCl and 90 mM LiCl).

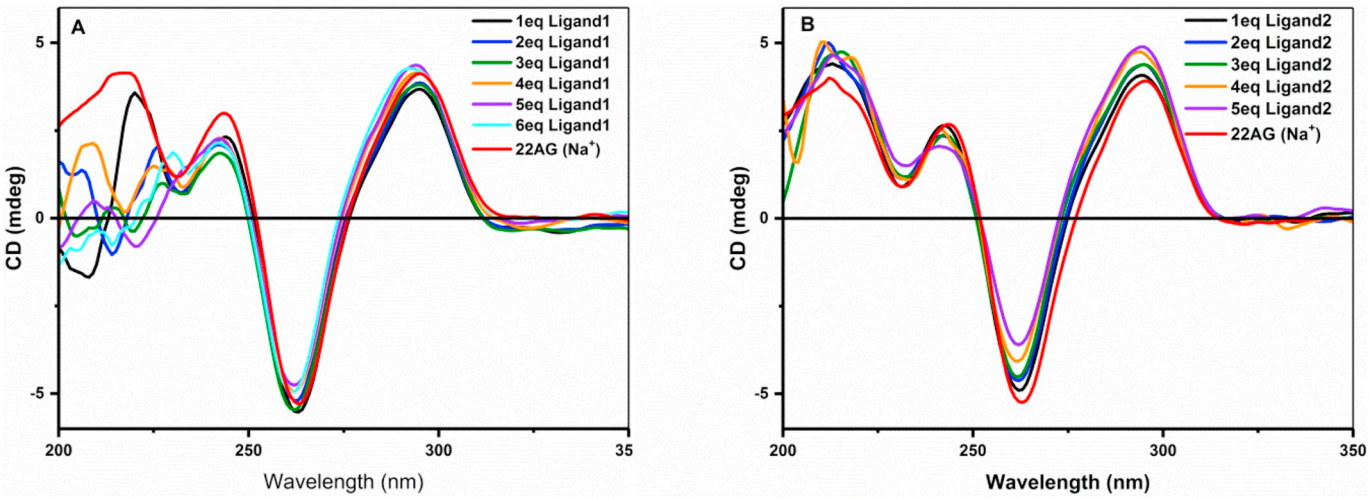

Fig. 4. CD titration spectra of 12.5 μM telomeric G4-DNA with ligand **1** and **2** in the presence of 10 mM lithium cacodylate buffer and 100 mM NaCl, pH 7.2 (A) Ligand **1**; and (B) Ligand **2**.

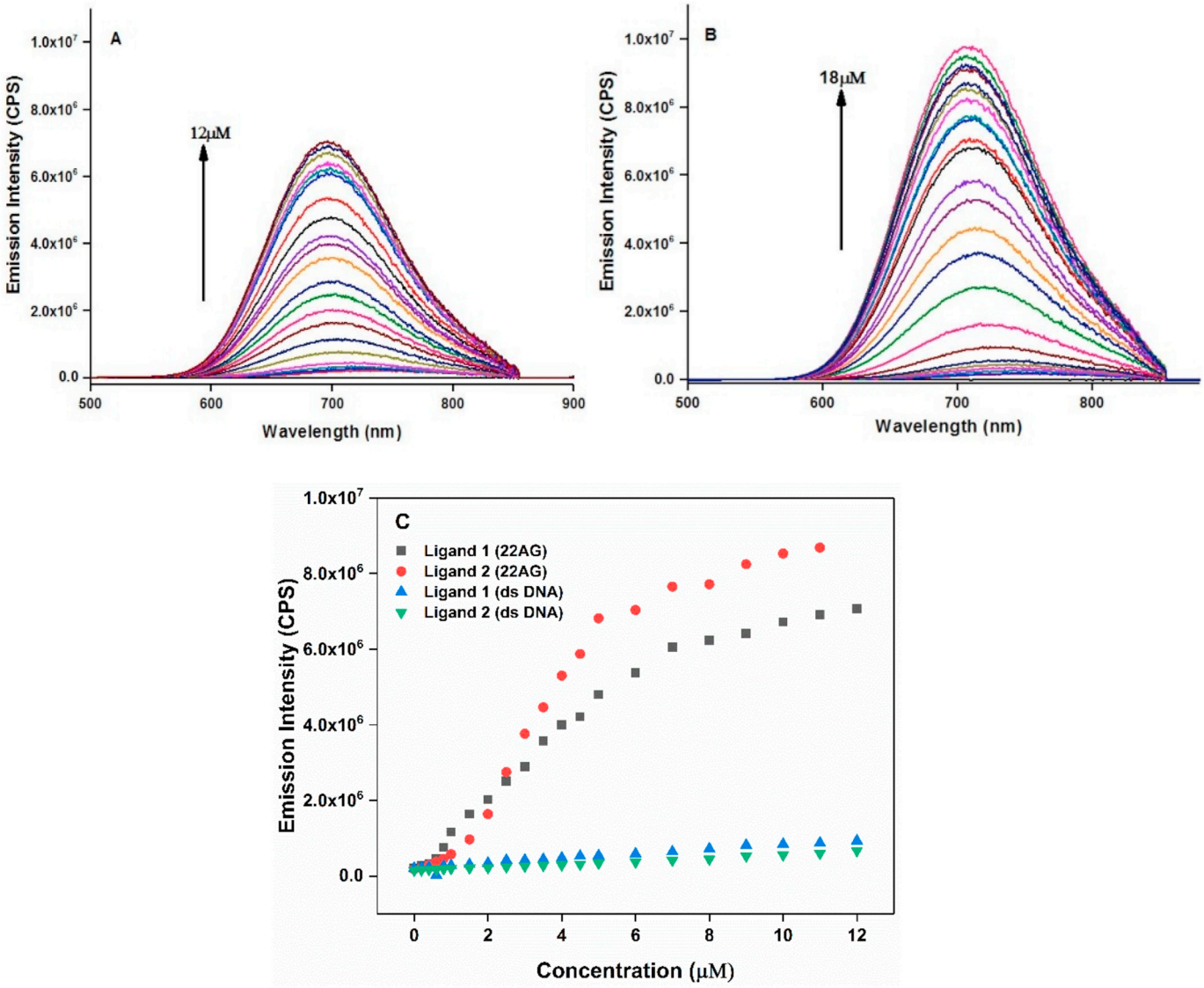

Fig. 5. Emission of ligands (10 μM, 100 mM NaCl and 10 mM lithium cacodylate buffer, pH 7.2) was titrated with telomeric (in similar salt and buffer conditions) A) Ligand **1** upto 12 μM of telomeric DNA and B) ligand **2** upto18 μM of telomeric DNA; C) A comparative plot of emission intensity changes of ligands **1** and **2** with increasing concentration with G4-DNA and ds-DNA.

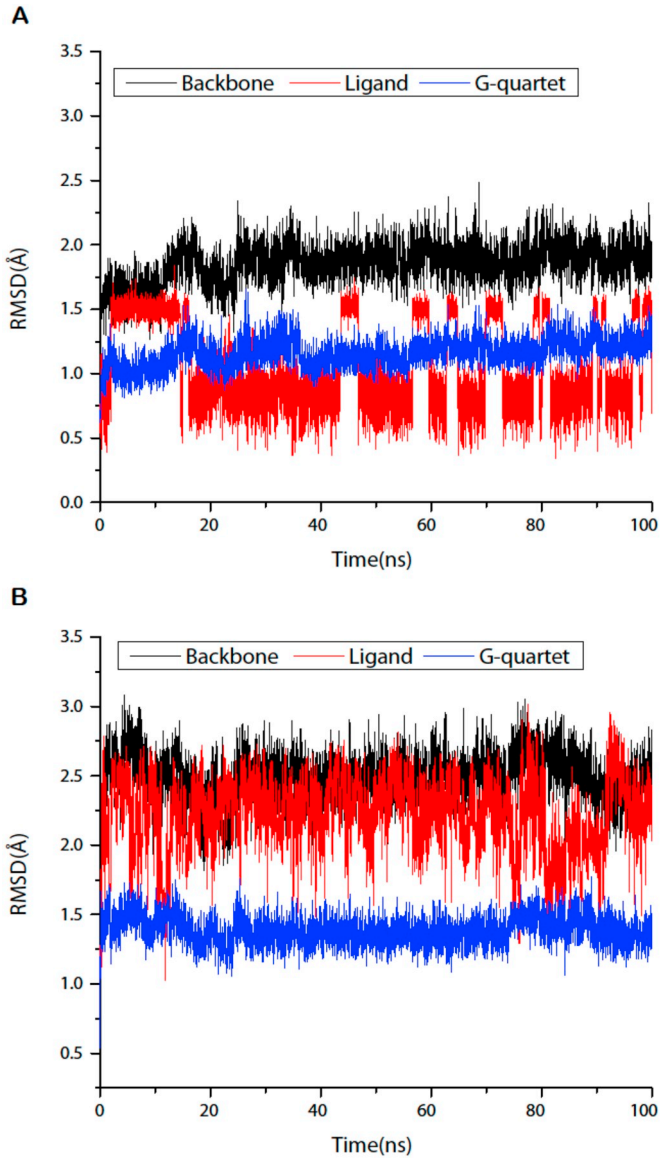

Fig. 6. Time-dependent root means square deviation (RMSD) plots of (A) ligand **1**/G4-DNA complex and (B) ligand **2**/G4-DNA complex. RMSDs of backbone atoms of DNA (black), G-quartets (blue) and ligand atoms (red) are plotted against time. Every 5th snapshot was taken, and a total of 10,000 frames were considered. (For interpretation of the references to colour in this figure legend, the reader is referred to the web version of this article.)

To get a qualitative overview of the general stability of the ligand-bound DNA complexes, the root mean square deviation (RMSD) values of atoms of the ligands, G-quartet and heavy atoms of the backbone concerning the first frame were plotted against time. From a visual and intuitive inspection of the nature of the RMSD plots, it is evident that the G-quartets are well stabilized in the presence of both ligands **1** and **2** [Fig. 6A and B]. The fluctuations in the RMSD plot of the backbone atoms were elucidated by the per-nucleotide root mean square fluctuation (RMSF) values of the loop residues in G4-DNA. All the guanine residues forming the quartets show lesser fluctuations than the other nucleotides [Fig. S5A and B]. Ligand **1** showed lower values of RMSDs when compared to ligand **2** due to the absence of the side chain. But it's orientation with respect to the G-quartet was found to be highly variable [Fig. S6]. Ligand **2** showed fluctuating RMSD values because of the dynamic nature of its side chain while ligand **1** showed lesser fluctuations, which arise mainly due to change in angles of the plane of the rings with respect to the chain. The average Hoogsteen H-bond occupancies of the G-quartets were found to be 94.2% for the ligand **1** and 93.6% for the ligand **2**.

Ligand **1** was very indiscriminate in the binding poses it adopted as there was no particular orientation, which was found favorable and stable in contrast to the behavior of ligand **2**. This could be reasoned out by the observation that none of the rings of ligand **1** was involved in any major stacking interactions, which were apparent in the final MD snapshots [Fig. 7A and B]. The naphthyl moiety was mostly positioned at the center of the top quartet while the pyridinium moiety interacts with the loop residues. This is in contrast to the situation of ligand (**2**) in which it was the ammonium cation of the side chain interacting with the backbone oxygen atoms. The pyridinium moiety of ligand **1** was observed to interact with the residues of the diagonal loop in such a way that it caused the carbonyl oxygen atoms of the thymine residues to reorient towards its positively charged pyridinium moiety. This is particularly observed for residue dT10 (Fig. S7). In the absence of any stacking interactions, ligand **1** is stabilized only by weak electrostatic forces. Ion-dipole interaction is observed between O4 of dT10 (average distance of 3.98 ± 0.44 Å) and pyridinium nitrogen of ligand **1** [Fig. S7 and S8].

Ligand **2** undergoes significant reorientation during the dynamics with the G4-DNA [Fig. S9]. This conformational flexibility gave an insight into possible interactions that cause the ligand to bind and stabilize the G4-DNA. From the different orientations adopted by ligand **2**, one particular orientation seemed to be quite favorable in terms of stacking and electrostatic interactions. Initially, ligand **2** does not stack over any of the bases and is held only by electrostatic interactions between the *N*-methyl ammonium cation and phosphate oxygens of flanking nucleotides. As the dynamics progressed, one of the naphthyl rings stack over dG1, while the pyridinium ring stacks partially over dG13 (Fig. S9B). A remarkable feature of the structure of ligand **2** is that the centre to centre distance of the naphthyl and pyridinium rings is around the same as that of the distance between centres of the rings of guanine residues 1 and 13 (Fig. S10). This facilitates efficient stacking interactions between the rings of ligand **2** and the top quartet. At around 80–90 ns, ligand **2** is hugely displaced from over the quartet to the edge, which eventually comes back to the stacked position over dG1 and dG13 as seen in the final snapshot (Fig. 7D). Stacking and electrostatic interactions seem to contribute significantly towards the stability of ligand **2** in complex with the G4-DNA. Quantitative estimation of stacking interactions based on the centre-to-centre distance between rings and angles between their planes are summarized in Table S2. Larger deviations from the mean values occur because of complete displacement of ligand **2** from the stacked position for around 10 ns of the simulation. But, as observed, the interactions persist for a significant 77% of the total simulation time. Including other minor stacking interactions, the naphthyl ring comes out to be the predominant contributor towards stacking. To probe the electrostatic interactions involved, the distance between the *N*-methylated ammonium atom from the side chain, N3 (marked in Fig. S4), of ligand **2** and neighbouring phosphate oxygen atoms of the G4-DNA backbone was examined. The distance plots between the nitrogen and oxygen atoms showed that N3 of ligand **2** shows electrostatic contacts on either side with OP2 of dG13 (average distance of 3.78 ± 0.15 Å) and OP2 of dG21 (average distance of 3.77 ± 0.15 Å). (Figs. S11 and S12). Owing to the steric crowding due to the bulky methyl group, the ligand doesn't stay in proximity to either atoms, and hence the average distances are relatively larger. These observations show that the ligand **2**/G4-DNA complex is more stable than that with ligand **1**.

To validate this, binding free energies of both the ligands with the G4-DNA were calculated using the MM-PBSA method [56]. The free energy components are listed in Table S3. The electrostatic contribution towards enthalpy in the case of ligand **2** is more as compared to ligand **1** because of the presence additional positive charge. But the entropy contribution results in almost similar binding free energies, slightly more favorable for the ligand **2** complex.

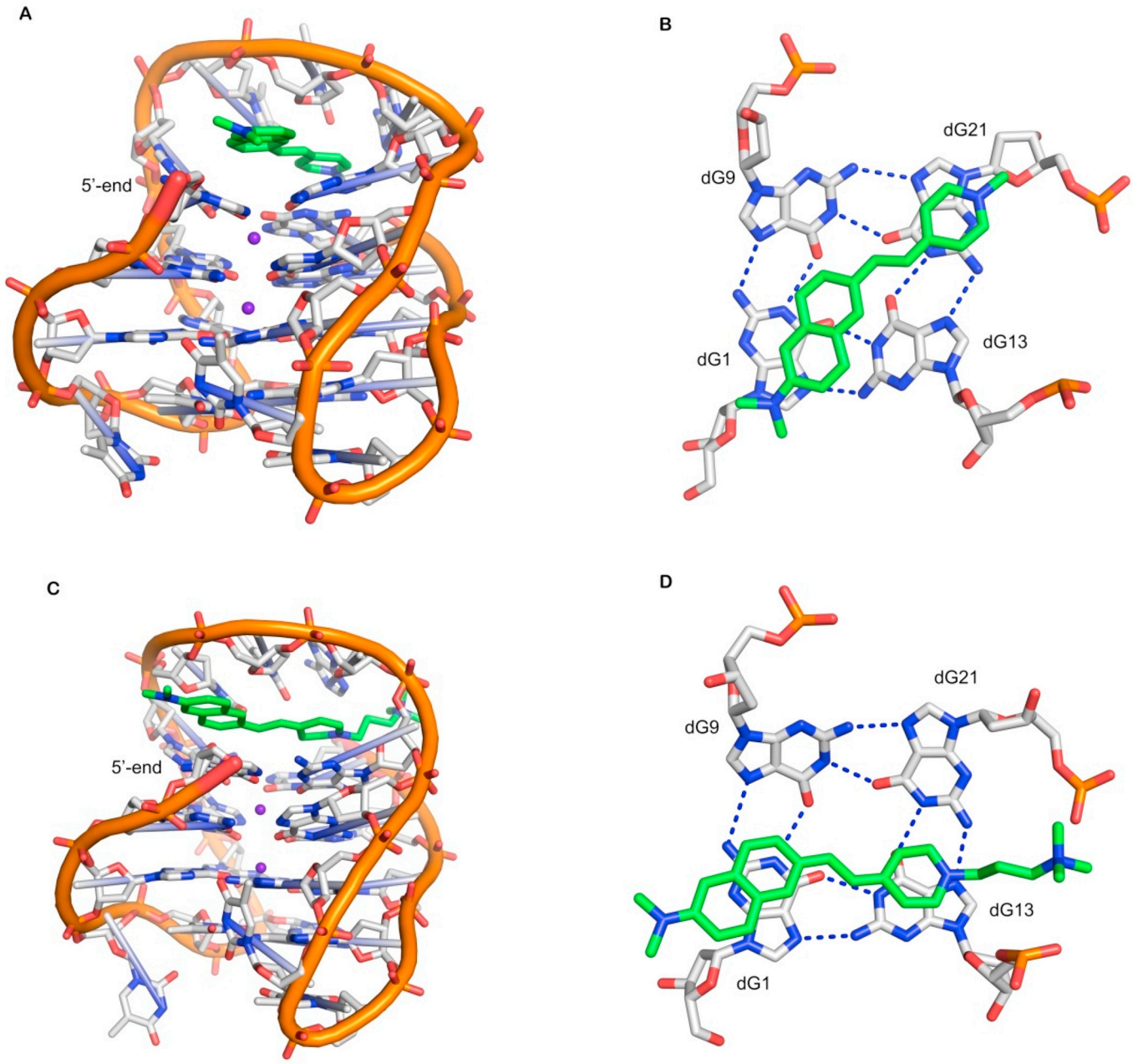

Fig. 7. Final MD snapshots of ligands **1** and **2** bound to antiparallel telomeric G4-DNA at the end of 100 ns simulations. Side views (left side) show the ligands bound onto the top quartet of G4-DNA. DNA and ligands are represented as sticks. The K^+ ions present in between the quartets are represented as violet spheres. Axial views (right side) show the ligand over the top quartet. Dashed lines show the hydrogen bonds present in the quartet. (A) side view of ligand **1** bound to G4-DNA (B) axial view of ligand **1** stacked over the top quartet (C) side view of ligand **2** bound to G4-DNA (D) axial view of ligand **2** over the top quartet. (For interpretation of the references to colour in this figure legend, the reader is referred to the web version of this article.)

8. Conclusions

In conclusion, we designed and synthesized water-soluble cationic styryl dyes bearing a dimethylamine donor and pyridinium acceptor groups and investigated their interactions with double-stranded and quadruplex DNAs. Owing to the presence of strong electron donating and electron withdrawing groups, the molecules show emission > 700 nm in aqueous media with a large Stokes shift. The presence of two positively charged groups in ligand **2** enables stronger binding affinity along with notable emission changes (~70 fold intensity enhancement) with G4-DNA. The water solubility, strong red-emission, preferential binding provide a promising scope for the development of fluorescent probes for targeting G4-DNAs having biological importance.

Acknowledgments

Authors acknowledge a financial grant from BRNS (Board of Research in Nuclear Sciences), India; 37(2)/14/05/2016) to S.K. and Science and Engineering Research Board (SERB-DST)-Government of India (Grant No. EMR/2016/003268) to P.I.P. Sushree S Pany acknowledges CSIR-New Delhi, Beena Kumari acknowledges IIT Gandhinagar for their fellowships. General infrastructural support from IIT Gandhinagar and IIT Bombay is acknowledged.

Appendix A. Supplementary data

Supplementary data to this article can be found online at https://doi.org/10.1016/j.jphotobiol.2018.10.007.

References

[1] S. Burge, G.N. Parkinson, P. Hazel, A.K. Todd, S. Neidle, Quadruplex DNA: sequence, topology and structure, Nucl. Acids Res. 34 (2006) 5402–5415.
[2] H.J. Lipps, D. Rhodes, G-quadruplex structures: *in vivo* evidence and function, *Trends Cell Biol.*, **19** 414–422.
[3] A. Siddiqui-Jain, C.L. Grand, D.J. Bearss, L.H. Hurley, Direct evidence for a G-quadruplex in a promoter region and its targeting with a small molecule to repress c-MYC transcription, Proc. Natl. Acad. Sci. U. S. A. 99 (2002) 11593–11598.
[4] L. Davis, N. Maizels, G4 DNA: at risk in the genome, EMBO J. 30 (2011) 3878–3879.
[5] S. Balasubramanian, L.H. Hurley, S. Neidle, Targeting G-quadruplexes in gene promoters: a novel anticancer strategy? Nat. Rev. Drug Discov. 10 (2011) 261–275.
[6] R. Rodriguez, K.M. Miller, J.V. Forment, C.R. Bradshaw, M. Nikan, S. Britton, T. Oelschlaegel, B. Xhemalce, S. Balasubramanian, S.P. Jackson, Small-molecule–induced DNA damage identifies alternative DNA structures in human genes, Nat. Chem. Biol. 8 (2012) 301–310.
[7] D.-L. Ma, Z. Zhang, M. Wang, L. Lu, H.-J. Zhong, C.-H. Leung, Recent developments in G-quadruplex probes, Chem. Biol. 22 (2015) 812–828.
[8] P. Agarwala, S. Pandey, S. Maiti, G-quadruplexes as tools for synthetic biology, Chembiochem 14 (2013) 2077–2081.
[9] A. Granzhan, H. Ihmels, N-Aryl-9-amino-substituted acridizinium derivatives as fluorescent “light-up” probes for DNA and protein detection, Org. Lett. 7 (2005) 5119–5122.
[10] H. Han, Q. Jin, H. Wang, W. Teng, J. Wu, H. Tong, T. Chen, J. Ji, Intracellular dual fluorescent light-up bioprobes for image-guided photodynamic cancer therapy, Small 12 (2016) 3870–3878.
[11] B.A. Armitage, Cyanine dye–DNA interactions: intercalation, groove binding, and aggregation, in: M.J. Waring, J.B. Chaires (Eds.), DNA Binders and Related Subjects, Springer Berlin Heidelberg, Berlin, Heidelberg, 2005, pp. 55–76.
[12] D. Bouzada, I. Salvado, G. Barka, G. Rama, J. Martinez-Costas, R. Lorca, A. Somoza, M. Melle-Franco, M.E. Vazquez, M. Vazquez Lopez, Selective G-quadruplex binding by oligoarginine-Ru(dppz) metallopeptides, Chem. Commun. 54 (2018) 658–661.
[13] G. Biffi, D. Tannahill, J. McCafferty, S. Balasubramanian, Quantitative visualization of DNA G-quadruplex structures in human cells, Nat. Chem. 5 (2013) 182–186.
[14] J. Mohanty, N. Barooah, V. Dhamodharan, S. Harikrishna, P.I. Pradeepkumar, A.C. Bhasikuttan, Thioflavin T as an efficient inducer and selective fluorescent sensor for the human telomeric G-quadruplex DNA, J. Am. Chem. Soc. 135 (2013) 367–376.
[15] A. Laguerre, L. Stefan, M. Larrouy, D. Genest, J. Novotna, M. Pirrotta, D. Monchaud, A twice-as-smart synthetic G-quartet: PyroTASQ is both a smart quadruplex ligand and a smart fluorescent probe, J. Am. Chem. Soc. 136 (2014) 12406–12414.
[16] P. Chilka, P.R. Patlolla, B. Datta, Selective recognition of G-quadruplexes by a dimeric carbocyanine dye, RSC Adv. 6 (2016) 87400–87404.
[17] J.-W. Yan, S.-B. Chen, H.-Y. Liu, W.-J. Ye, T.-M. Ou, J.-H. Tan, D. Li, L.-Q. Gu, Z.-S. Huang, Development of a new colorimetric and red-emitting fluorescent dual probe for G-quadruplex nucleic acids, Chem. Commun. 50 (2014) 6927–6930.
[18] S.-B. Chen, M.-H. Hu, G.-C. Liu, J. Wang, T.-M. Ou, L.-Q. Gu, Z.-S. Huang, J.-H. Tan, Visualization of NRAS RNA G-quadruplex structures in cells with an engineered fluorogenic hybridization probe, J. Am. Chem. Soc. 138 (2016) 10382–10385.
[19] X.-C. Chen, S.-B. Chen, J. Dai, J.-H. Yuan, T.-M. Ou, Z.-S. Huang, J.-H. Tan, Tracking the dynamic folding and unfolding of RNA G-quadruplexes in live cells, Angew. Chem. Int. Ed. 57 (2018) 4702–4706.
[20] Y.-Q. Wang, M.-H. Hu, R.-J. Guo, S.-B. Chen, Z.-S. Huang, J.-H. Tan, Tuning the selectivity of a commercial cyanine nucleic acid dye for preferential sensing of hybrid telomeric G-quadruplex DNA, Sens. Act. B 266 (2018) 187–194.
[21] A. Shivalingam, M.A. Izquierdo, A.L. Marois, A. Vyšniauskas, K. Suhling, M.K. Kuimova, R. Vilar, The interactions between a small molecule and G-quadruplexes are visualized by fluorescence lifetime imaging microscopy, Nat. Commun. 6 (2015) 8178.
[22] H. Lai, Y. Xiao, S. Yan, F. Tian, C. Zhong, Y. Liu, X. Weng, X. Zhou, Symmetric cyanovinyl-pyridinium triphenylamine: a novel fluorescent switch-on probe for an antiparallel G-quadruplex, Analyst 139 (2014) 1834–1838.
[23] A.C. Bhasikuttan, J. Mohanty, Targeting G-quadruplex structures with extrinsic fluorogenic dyes: promising fluorescence sensors, Chem. Commun. 51 (2015) 7581–7597.
[24] F. Doria, M. Nadai, M. Zuffo, R. Perrone, M. Freccero, S.N. Richter, A red-NIR fluorescent dye detecting nuclear DNA G-quadruplexes: in vitro analysis and cell imaging, Chem. Commun. 53 (2017) 2268–2271.
[25] M. Balazy, A. Fausto, C. Voskanian, B. Chavez, H. Panesar, T.G. Minehan, Dimeric and trimeric derivatives of the azinomycin B chromophore show enhanced DNA binding, Org. Biomol. Chem. 15 (2017) 4522–4526.
[26] M. Zuffo, S. Ladame, F. Doria, M. Freccero, Tuneable coumarin-NDI dyads as G-quadruplex specific light-up probes, Sens. Act. B 245 (2017) 780–788.
[27] F. Doria, A. Oppi, F. Manoli, S. Botti, N. Kandoth, V. Grande, I. Manet, M. Freccero, A naphthalene diimide dyad for fluorescence switch-on detection of G-quadruplexes, Chem. Commun. 51 (2015) 9105–9108.
[28] A. Spinello, G. Barone, J. Grunenberg, Molecular recognition of naphthalene diimide ligands by telomeric quadruplex-DNA: the importance of the protonation state and mediated hydrogen bonds, Phys. Chem. Chem. Phys. 18 (2016) 2871–2877.
[29] R.X.F. Ren, N.C. Chaudhuri, P.L. Paris, S. Rumney, E.T. Kool, Naphthalene, phenanthrene, and pyrene as DNA base analogues: synthesis, structure, and fluorescence in DNA, J. Am. Chem. Soc. 118 (1996) 7671–7678.
[30] P. Verwilst, H.-R. Kim, J. Seo, N.-W. Sohn, S.-Y. Cha, Y. Kim, S. Maeng, J.-W. Shin, J.H. Kwak, C. Kang, J.S. Kim, Rational design of in vivo tau tangle-selective near-infrared fluorophores: expanding the BODIPY universe, J. Am. Chem. Soc. 139 (2017) 13393–13403.
[31] S. Singha, Y.W. Jun, J. Bae, K.H. Ahn, Ratiometric imaging of tissue by two-photon microscopy: observation of a high level of formaldehyde around mouse intestinal crypts, Anal. Chem. 89 (2017) 3724–3731.
[32] H. Fu, P. Tu, L. Zhao, J. Dai, B. Liu, M. Cui, Amyloid-β deposits target efficient near-infrared fluorescent probes: synthesis, in vitro evaluation, and in vivo imaging, Anal. Chem. 88 (2016) 1944–1950.
[33] S. Haider, S. Neidle, Molecular modeling and simulation of G-quadruplexes and quadruplex-ligand complexes, G-Quadruplex DNA, Springer, 2010, pp. 17–37.
[34] V. Dhamodharan, S. Harikrishna, C. Jagadeeswaran, K. Halder, P.I. Pradeepkumar, Selective G-quadruplex DNA stabilizing agents based on bisquinolinium and bispyridinium derivatives of 1, 8-naphthyridine, J. Org. Chem. 77 (2011) 229–242.
[35] E. Vanquelef, S. Simon, G. Marquant, E. Garcia, G. Klimerak, J.C. Delepine, P. Cieplak, F.-Y. Dupradeau, R.E.D. Server: a web service for deriving RESP and ESP charges and building force field libraries for new molecules and molecular fragments, Nucl. Acids Res. 39 (2011) W511–W517.
[36] G.M. Morris, D.S. Goodsell, R.S. Halliday, R. Huey, W.E. Hart, R.K. Belew, A.J. Olson, Automated docking using a Lamarckian genetic algorithm and an empirical binding free energy function, J. Comput. Chem. 19 (1998) 1639–1662.
[37] J. Wang, R.M. Wolf, J.W. Caldwell, P.A. Kollman, D.A. Case, Development and testing of a general amber force field, J. Comput. Chem. 25 (2004) 1157–1174.
[38] M. Zgarbová, M. Otyepka, J.i. Šponer, A.t. Mládek, P. Banáš, T.E. Cheatham, P. Jurecka, Refinement of the Cornell et al. nucleic acids force field based on reference quantum chemical calculations of glycosidic torsion profiles, J. Chem. Theory Comput. 7 (2011) 2886–2902.
[39] T. Fox, P.A. Kollman, Application of the RESP methodology in the parametrization of organic solvents, J. Phys. Chem. B 102 (1998) 8070–8079.
[40] A.W.S. da Silva, W.F. Vranken, ACPYPE-antechamber python parser interface, BMC Res. Notes 5 (2012) 367.
[41] R. Salomon-Ferrer, A.W. Götz, D. Poole, S. Le Grand, R.C. Walker, Routine microsecond molecular dynamics simulations with AMBER on GPUs. 2. Explicit solvent particle mesh Ewald, J. Chem. Theory Comput. 9 (2013) 3878–3888.
[42] A.W. Götz, M.J. Williamson, D. Xu, D. Poole, S. Le Grand, R.C. Walker, Routine microsecond molecular dynamics simulations with AMBER on GPUs. 1. Generalized born, J. Chem. Theory Comput. 8 (2012) 1542–1555.
[43] P.A. Kollman, I. Massova, C. Reyes, B. Kuhn, S. Huo, L. Chong, M. Lee, T. Lee, Y. Duan, W. Wang, Calculating structures and free energies of complex molecules: combining molecular mechanics and continuum models, Acc. Chem. Res. 33 (2000) 889–897.
[44] D.R. Roe, T.E. Cheatham Iii, PTRAJ and CPPTRAJ: software for processing and analysis of molecular dynamics trajectory data, J. Chem. Theory Comput. 9 (2013) 3084–3095.
[45] E.F. Pettersen, T.D. Goddard, C.C. Huang, G.S. Couch, D.M. Greenblatt, E.C. Meng, T.E. Ferrin, UCSF Chimera—a visualization system for exploratory research and analysis, J. Comput. Chem. 25 (2004) 1605–1612.
[46] X. Gao, Y. Zhang, B. Wang, A highly fluorescent water-soluble boronic acid reporter for saccharide sensing that shows ratiometric UV changes and significant fluorescence changes, Tetrahedron 61 (2005) 9111–9117.
[47] D.J. Hayne, A.J. North, M. Fodero-Tavoletti, J.M. White, L.W. Hung, A. Rigopoulos, C.A. McLean, P.A. Adlard, U. Ackermann, H. Tochon-Danguy, Rhenium and technetium complexes that bind to amyloid-β plaques, Dalton Trans. 44 (2015) 4933–4944.
[48] P. Yan, A. Xie, M. Wei, L.M. Loew, Amino (oligo) thiophene-based environmentally sensitive biomembrane chromophores, J. Org. Chem. 73 (2008) 6587–6594.
[49] A. Petrič, S.A. Johnson, H.V. Pham, Y. Li, S. Čeh, A. Golobič, E.D. Agdeppa, G. Timbol, J. Liu, G. Keum, N. Satyamurthy, V. Kepe, K.N. Houk, J.R. Barrio, Dicyanovinylnaphthalenes for neuroimaging of amyloids and relationships of electronic structures and geometries to binding affinities, Proc. Natl. Acad. Sci. U. S. A 109 (2012) 16492–16497.
[50] A. Cañete, M.X. Meléndrez, C. Saitz, A.L. Zanocco, Synthesis of aminonaphthalene derivatives using the bucherer reaction under microwave irradiation, Syn. Commun. 31 (2001) 2143–2148.
[51] A.S. Rao, D. Kim, T. Wang, K.H. Kim, S. Hwang, K.H. Ahn, Reaction-based two-photon probes for mercury ions: fluorescence imaging with dual optical windows, Org. Lett. 14 (2012) 2598–2601.
[52] J.-T. Hou, J. Yang, K. Li, Y.-X. Liao, K.-K. Yu, Y.-M. Xie, X.-Q. Yu, A highly selective water-soluble optical probe for endogenous peroxynitrite, Chem. Commun. 50 (2014) 9947–9950.
[53] P. Jana, M. Radhakrishna, S. Khatua, S. Kanvah, A “turn-off” red-emitting fluorophore for nanomolar detection of heparin, Phys. Chem. Chem. Phys. 20 (2018) 13263–13270.
[54] D. Miyoshi, A. Nakao, N. Sugimoto, Structural transition from antiparallel to parallel G-quadruplex of d (G4T4G4) induced by Ca2+, Nucl. Acids Res. 31 (2003) 1156–1163.
[55] Y. Wang, D.J. Patel, Solution structure of the human telomeric repeat d [AG3(T2AG3)3] G-tetraplex, Structure 1 (1993) 263–282.
[56] S. Genheden, U. Ryde, The MM/PBSA and MM/GBSA methods to estimate ligand-binding affinities, Expert Open Drug Discov. 10 (2015) 449–461.